

Synthetic Methods

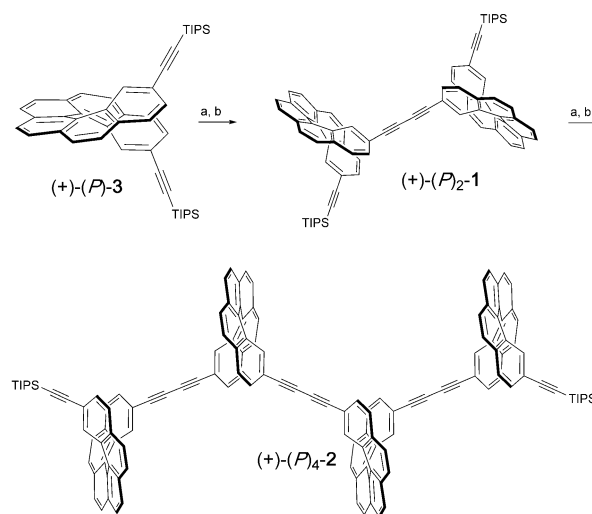
Helical Threads: Enantiomerically Pure Carbo[6]Helicene Oligomers

Cédric Schaack, Eric Sidler, Nils Trapp, and François Diederich*^[a]

Abstract: We report the synthesis of enantiomerically pure carbo[6]helicene oligomers with buta-1,3-diyne-1,4-diyl bridges between the helicene nuclei. The synthesis of monomeric (\pm)-2,15-bis[(triisopropylsilyl)ethynyl]carbo[6]helicene was achieved in 25% yield over six steps. Pure (+)-(*P*)- and (–)-(*M*)-enantiomers were obtained by HPLC on a chiral stationary phase. The dimeric (+)-(*P*)₂- and (–)-(*M*)₂-configured and the tetrameric (+)-(*P*)₄- and (–)-(*M*)₄-configured oligomers were obtained by sequential oxidative acetylenic coupling. The ECD spectra of the tetrameric oligomers displayed large Cotton effect intensities of $\Delta\epsilon = -851 \text{ M}^{-1} \text{ cm}^{-1}$ at $\lambda = 370 \text{ nm}$ ((*M*)₄-enantiomer). We transformed the buta-1,3-diyne-1,4-diyl bridge in the dimeric (*P*)₂ and (*M*)₂ oligomer by heteroaromatization into a thiene-2,5-diyl linker. Although the resulting chromophore showed reduced ECD intensities, it exhibited a remarkably strong fluorescence emission at 450–500 nm, with an absolute quantum yield of 25%.

Carbo[*n*]helicenes are polyaromatic hydrocarbons (PAH) featuring a helical, π -conjugated backbone, which imparts inherent chirality and strong chiroptical responses.^[1] Elongation of the helical backbone has been intensively pursued,^[2] culminating in the recent synthesis of a carbo[16]helicene by Fujita and co-workers.^[3] More recently, fused helicenes have been incorporated into nanographenes, breaking the planarity of the carbon sheets and enhancing their processability.^[4] Yamaguchi and co-workers reported the first acyclic and macrocyclic helicene oligomers, based on 1,12-dimethylbenzo[*c*]phenanthrene monomers linked by ethyne-1,2-diyl moieties.^[5] These [4]helicene-containing macromolecules showed strong chiroptical responses while suffering from aggregation in solution. In 2013, our group reported the first ethene-1,2-diyl-linked (*P*)₂- and (*M*)₂-configured [6]helicene dimers.^[6] The unexpectedly intense

chiroptical properties displayed by these dimeric systems were found to originate from an increase in the π -conjugated chromophore surface. Encouraged by these findings, we report herein the synthesis and properties of enantiopure dimeric ((*P*)₂-1 and (*M*)₂-1) and tetrameric ((*P*)₄-2 and (*M*)₄-2) [6]helicene oligomers, in which the helicene nuclei are connected by buta-1,3-diyne-1,4-diyl linkers in a linear fashion (Scheme 1). We show that the buta-1,3-diyne-1,4-diyl linker in the dimeric systems can be transformed by heteroaromatization into a thiophene ring, and investigated the interesting photophysical properties of the resulting thiene-2,5-diyl-linked dimeric [6]helicene.^[7] Additionally, building on the many theoretical studies performed on helicene scaffolds,^[8] we fully supplemented the experimental spectroscopic study by density functional theory (DFT) calculations, providing further insight into the measured electronic circular dichroism (ECD) and UV/Vis spectra.



Scheme 1. Synthesis of dimeric (*P*)₂-1 and tetrameric (*P*)₄-2 from enantiopure (*P*)-3. Reagents and conditions: a) TBAF (0.7 equiv), MeOH/THF (1:5), 22 °C, 72 h, 30% ((*P*)-4) and 21% ((*P*)₂-5); b) CuI (10% mol), [Pd(PPh₃)₂Cl₂] (10% mol), TMEDA, toluene, 22 °C, 14 h, 89% (for the formation of (*P*)₂-1) and 45% (for the formation of (*P*)₄-2). TBAF = tetrabutylammonium fluoride, TMEDA = tetramethylethylenediamine.

Racemic 2,15-bis[(triisopropylsilyl)ethynyl]carbo[6]helicene (\pm)-3 was prepared in 25% over six steps according to known procedures (Section S1 in the Supporting Information) and subsequently resolved by preparative HPLC on a chiral stationary phase (Pirkle-type Regis Technologies (*S,S*)-Whelk-O 1, hexane/CHCl₃ 98:2, see Section S2 in the Supporting Informa-

[a] C. Schaack, E. Sidler, Dr. N. Trapp, Prof. Dr. F. Diederich
Laboratorium für Organische Chemie, ETH Zurich
Hönggerberg, HCI, Vladimir-Prelog-Weg 3
8093 Zurich (Switzerland)
E-mail: diederich@org.chem.ethz.ch

Supporting information and the ORCID identification number(s) for the author(s) of this article can be found under <https://doi.org/10.1002/chem.201703024>. It contains the synthetic procedures for all compounds and their ¹H and ¹³C NMR spectra, crystal-structure data for compounds (\pm)-3, (–)-(*M*)₂-1, (–)-(*M*)₂-6 and (+)-(*P*)₂-6, as well as other various intermediates, details on the DFT calculations, and HPLC separation data and chromatograms.

tion). The absolute configuration was unambiguously confirmed by X-ray crystallography and ECD spectroscopy, coupled with DFT calculations (B3LYP/6-31G(d)^[9]). Consistent with previous reports, the longest-wavelength band exhibits a positive Cotton effect for the first, and a negative Cotton effect for the second eluting fraction (see Figure 2 for ECD spectra and Section S4 in the Supporting Information for the X-Ray crystal structures).^[10,11] Subsequent measurement of the specific rotation confirmed that the first eluted fraction at retention time $t_R = 6.6$ min corresponded to the (*P*)-enantiomer, whereas the second eluted fraction at $t_R = 11.0$ min gave the (*M*)-enantiomer.

Selective cleavage of one triisopropylsilyl group in (*P*)-**3** by using tetrabutylammonium fluoride (0.7 equiv) gave singly deprotected (*P*)-**4** (not shown, see the Supporting Information) in 30% yield, while recovering 60% of (*P*)-**3**. Pd-catalyzed oxidative homocoupling by using [Pd(PPh₃)₂Cl₂] and CuI gave (*P*)₂-**1** in high yield (89%; Scheme 1).^[12] The enantiomeric purity of this compound was ascertained by HPLC on a chiral stationary phase (see Chapter S2 in the Supporting Information) and further confirmed by X-ray analysis (see Chapter S4 in the Supporting Information).

The crystal structure of (*M*)₂-**1** (space group *P*2₁) shows a dihedral angle of 34° between the two benzene rings that are connected by the buta-1,3-diyne-1,4-diyl linker, with both helicenes placed on opposite sides of this fragment (Figure 1). A

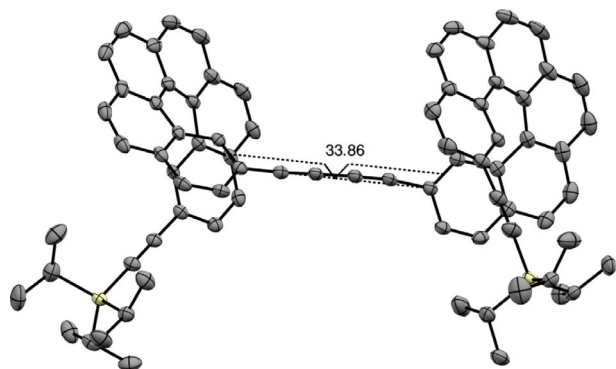


Figure 1. ORTEP plot of (*M*)₂-**1**. Hydrogen atoms have been omitted for clarity. Atomic displacement ellipsoids at 100 K are drawn at the 50% probability level. Further information on bond lengths [Å] and torsions [°] can be found in the Supporting Information.

polymorph of (*M*)₂-**1** with the space group *P*2₁2₁2₁, showed an angle of -57°, with both helicenes rotating to the same side of the diphenylbutadiyne fragment. In contrast, the *meso*, (*M,P*)-configured dimer (*M,P*)-**1** with the space group $\bar{P}1$ showed a flat diphenylbutadiyne fragment with an interplanar angle of 0° (see Section S4 in the Supporting Information). DFT calculations gave a barrier for rotation of the two benzene rings attached to the buta-1,3-diyne-1,4-diyl moiety of only 0.7 kcal mol⁻¹ (DFT:B3LYP/6-31G(d)), with the highest-energy conformation displaying a 91° angle between the two rings (Section S3.3 in the Supporting Information).

Monodeprotection of (*P*)₂-**1** and (*M*)₂-**1** afforded singly deprotected (*P*)₂-**5** and (*M*)₂-**5** (not shown, see the Supporting Information) in 21% and 35% yield, respectively. Subsequent oxidative Glaser–Eglinton coupling yielded the tetrameric (*P*)₄- and (*M*)₄-configured oligomers in 45% and 27% yield, respectively (Scheme 1).

The chiroptical properties of the enantiomerically pure mono-, di-, and tetrameric helicenes are shown in Figure 2. UV/Vis absorbance and Cotton effect intensities of monomeric (*P*)-**3** and (*M*)-**3** were consistent with previously reported

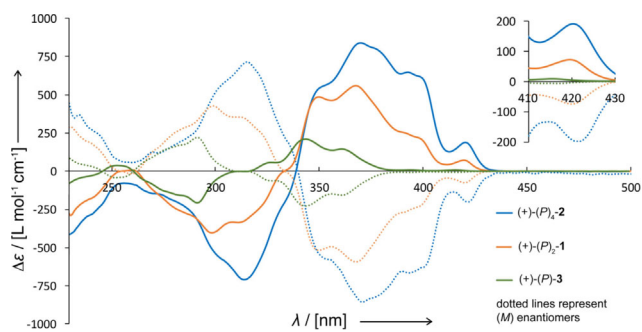


Figure 2. ECD spectra of monomeric **3** (green lines), dimeric **1** (orange line), and tetrameric **2** (blue line) measured at $c = 10^{-6}$ M in CH₂Cl₂ at 296 K. Dashed lines correspond to the (*M*)_n-enantiomers, solid lines to the (*P*)_n-enantiomers ($n = 1, 2, 4$). The inset shows a magnified view of the band in the 410–430 nm region.

values for related compounds (Figure 3).^[8c,d] Similarly to the previously reported dimeric, ethene-1,2-diyl-linked [6]helicene,^[6] (*M*)₂-**1** and (*P*)₂-**1** show a non-linear increase in Cotton effects compared to (*M*)-**3** and (*P*)-**3**, respectively, accompanied by a bathochromic shift of the ¹B_b band^[13] maxima (λ_{max}) by 23 nm (Table 1).

To the best of our knowledge, tetrameric helicene (*P*)₄-**2** and (*M*)₄-**2** show the highest Cotton effect for any [6]helicene-based chromophoric system reported to date, with $\Delta\epsilon = 842$ M⁻¹ cm⁻¹ at $\lambda = 371$ nm for the (*P*)₄-enantiomer, a fourfold increase in intensity compared to monomeric (*P*)-**3** and (*M*)-**3**. However, there is no more non-linear increase in Cotton band intensity from dimeric to tetrameric oligomer, and the intensity is not even doubled, as expected for a linear increase from the

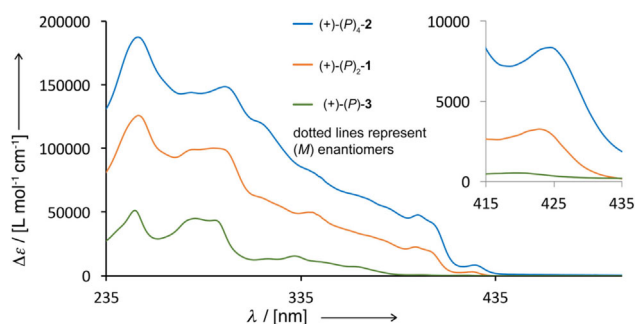


Figure 3. UV/Vis spectra of monomeric **3** (green lines), dimeric **1** (orange line), and tetrameric **2** (blue line) measured at $c = 10^{-6}$ M in CH₂Cl₂ at 296 K. The inset shows a magnified view of the band in the 410–430 nm region.

Table 1. Summary of the $\Delta\epsilon$ values of the 1B_b bands for both enantiomers of monomeric **3**, dimeric **1**, and tetrameric **2**, and the thiene-2,5-diyl-bridged dimeric **6**, recorded in CH_2Cl_2 at concentrations at $c \approx 10^{-6}$ [mol L $^{-1}$] in CH_2Cl_2 at 296 K.

Compound	$\Delta\epsilon$ [L mol $^{-1}$ cm $^{-1}$]	λ_{max} [nm]
(<i>P</i>)- 3	209	344
(<i>M</i>)- 3	-220	345
(<i>P</i>) $_2$ - 1	561	368
(<i>M</i>) $_2$ - 1	-579	367
(<i>P</i>) $_4$ - 2	842	371
(<i>M</i>) $_4$ - 2	-851	370
(<i>P</i>) $_2$ - 6	332	364
(<i>M</i>) $_2$ - 6	-283	363

doubling of the number of helicene nuclei. Additionally, the λ_{max} values for the 1B_b bands of the tetrameric system only show a modest bathochromic shift of 3 nm (Table 1). Interestingly, the second 1B_b band^[13] of tetrameric **2** displays a Cotton effect of $\Delta\epsilon = 716 \text{ M}^{-1} \text{ cm}^{-1}$ at $\lambda_{\text{max}} = 314 \text{ nm}$, which corresponds to a substantial bathochromic shift and intensity increase compared to dimeric **1** ($\Delta\epsilon = 426 \text{ M}^{-1} \text{ cm}^{-1}$ at $\lambda_{\text{max}} = 299 \text{ nm}$).

The increase in the number of helicene nuclei in the oligomers comes with a linear increase in specific and molar optical rotations. Indeed, the molar optical rotation doubled from $[\phi]_{\text{D}}^{23} = 18\,125$ [$^\circ \text{ cm}^2 \text{ dmol}^{-1}$] in (*P*)-**3** to $40\,767$ [$^\circ \text{ cm}^2 \text{ dmol}^{-1}$] in (*P*) $_2$ -**1** and again to $82\,084$ [$^\circ \text{ cm}^2 \text{ dmol}^{-1}$] in (*P*) $_4$ -**2**. Such a linear increase had already been previously reported for bis-helicenic terpyridine systems by Crassous and co-workers.^[14]

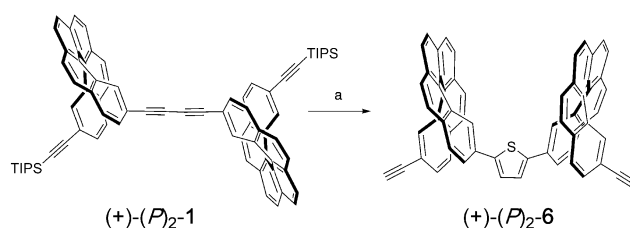
The UV/Vis spectra showed a 2.7-fold increase of the intensity from (*M*)-**3** to (*M*) $_2$ -**1** (Figure 3). Tetrameric (*M*) $_4$ -**2** (blue line) showed another large increase in UV/Vis intensity, although less than a doubling of the Cotton effect is seen upon changing from dimeric (*M*) $_2$ -**1** to tetrameric (*M*) $_4$ -**2**. The *g*-factor ($g = \Delta\epsilon/\epsilon$) plots display strong similarities for all three oligomers between 240 and 360 nm (Figure S4 in the Supporting Information). However, the tetrameric chromophores exhibit a three-fold higher *g*-factor intensity at 422 nm, originating from the new band that appears in the ECD (inset in Figure 2) and UV/Vis (inset in Figure 3) spectra.

DFT calculations of ECD and UV/Vis spectra were performed by using Gaussian 09^[9] (Section S3 in the Supporting Information). Structures were optimized at the B3LYP/6-31G(d) level of theory, with the TIPS replaced by TMS groups. ECD spectra for the lowest-energy conformer of each of (*P*)-**3**, (*M*) $_2$ -**1** and (*M*) $_4$ -**2** were calculated at the TD-DFT:cam-B3LYP/6-31G(d) level of theory incorporating 72 states. A comparison between experimental and theoretical spectra showed good agreement (Section S3 in the Supporting Information).

We also calculated the highest occupied (HOMO) and lowest unoccupied (LUMO) orbitals (B3LYP/6-31G(d); the accuracy of this basis set was confirmed by comparison with B3LYP/DGTVZVP for tetrameric (*P*) $_4$ -**2**; Section S3.2 in the Supporting Information). In dimeric (*P*) $_2$ -**1**, the electronic density of these orbitals was fully delocalized over both helicene moieties. In contrast, in tetrameric (*P*) $_4$ -**2**, a clear loss in delocalization can

be seen. The HOMO and LUMO are no longer delocalized over the whole molecule, but are mostly localized on the central dimeric helicene core. It is tempting to correlate these changes in delocalization of the HOMO/LUMO orbitals to the experimentally observed chiroptical properties, although other effects, such as differences in charge-transfer states, may also contribute. A greatly increased π -electron delocalization in the dimeric chromophore leads to non-linear increase of the ECD band intensities, compared to the monomer.^[6] Subsequent reduction in π -electron delocalization in the tetrameric chromophore gave a much weaker increase in intensity of the Cotton effects.

We subjected (*P*) $_2$ -**1** to heteroaromatization conditions with Na_2S in DMSO/THF 1:1 in the presence of KOH (Scheme 2).^[7c,d] Quantitative conversion to thiene-2,5-diyl-linked (*P*) $_2$ -**6** occurred, as was evidenced by the ${}^1\text{H}$ NMR spectra of the crude



Scheme 2. Quantitative cyclocondensation of the buta-1,3-diyne-1,4-diyl moiety in (*P*) $_2$ -**1** with Na_2S with simultaneous cleavage of the TIPS groups affords thiene-2,5-diyl-linked (*P*) $_2$ -**6**. Reagent and conditions: KOH (0.3 equiv), $\text{Na}_2\text{S}\cdot 9\text{H}_2\text{O}$ (2 equiv), DMSO/THF 1:1, 80 $^\circ\text{C}$, 1.5 h, quant. (isolated yield = 96%).

material. Remarkably, both TIPS groups were cleaved under the basic conditions. The longest-wavelength Vis absorptions of (*P*) $_2$ -**6** are substantially bathochromically shifted (by 12 nm) compared to the absorptions of the buta-1,3-diyne-1,4-diyl-bridged dimer (*P*) $_2$ -**1** (Figure S5 in the Supporting Information). The thiophene-linked dimer exhibited fluorescence under laboratory UV light at 365 nm, and we further explored this desirable property, which is quite rare for carbohelicenes with unsubstituted all-benzene backbones.^[15] The compound shows a structured emission band between 440 and 580 nm with two maxima at $\lambda_{\text{em}} = 457$ and 481 nm, attributed to the S_0 symmetrical vibrational mode.^[15a] The absolute fluorescence quantum yield^[16] is 0.25 at $\lambda_{\text{exc}} = 400 \text{ nm}$ (Figure 4). Monomeric (*P*)-**3**, buta-1,3-diyne-1,4-diyl-linked dimeric (*P*) $_2$ -**1**, and tetrameric (*P*) $_4$ -**2** showed expectedly low absolute fluorescence quantum yields of 0.04, 0.1, and 0.06, respectively, with the emission band ($\lambda_{\text{em}} = 420$ and 454 nm) also indicative of the S_0 vibrational mode (Figure S3 in the Supporting Information). ECD (Figure S6 in the Supporting Information) and UV/Vis spectral intensities of the thiophene-bridged dimer (*P*) $_2$ -**6** were moderately lower than those of (*P*) $_2$ -**1**.

A DFT investigation of the HOMO and LUMO orbitals of (*P*) $_2$ -**6** revealed that the density of the HOMO is localized around the thiophene core. In the LUMO state, this trend is reversed, showing little density on the central thiophene, but on the outer helicene benzene rings instead. This picture resem-

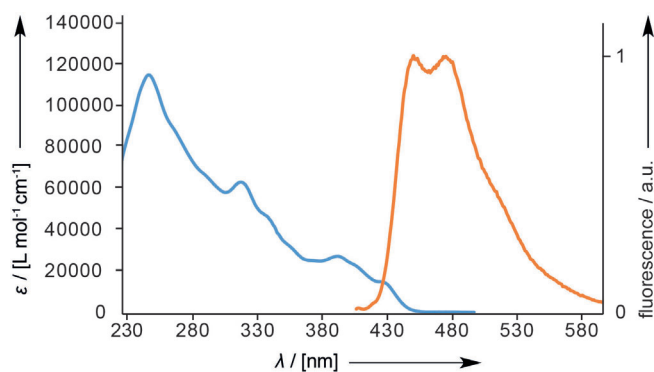


Figure 4. UV/Vis spectrum (blue line) and emission spectrum (orange line) ($\lambda_{exc} = 400$ nm) of $(P)_2\text{-6}$ measured at $c = 10^{-6}$ M in CH_2Cl_2 at 296 K. The fluorescence spectrum is given in arbitrary units. Identical features were measured for $(M)_2\text{-6}$ (see Figure S5 in the Supporting Information).

bles that for intermolecular non-planar push/pull chromophores^[17] and suggests that the thiophene ring acts as a donor and the helicene nuclei as the acceptors, in agreement with the bathochromic shift of the longest-wavelength Vis band (see Figure S5 in the Supporting Information).

Crystallization of $(M)_2\text{-6}$ afforded two solvomorphs: Vapor diffusion of *n*-hexane into a CH_2Cl_2 solution of the helicene gave $(M)_2\text{-6} \cdot 0.5\text{CH}_2\text{Cl}_2$ in space group $C222_1$ (Figure 5), while vapor diffusion of MeCN into CH_2Cl_2 gave $(M)_2\text{-6} \cdot \text{MeCN}$ in space group $P6_522$. The structures of the same solvates of enantiomeric $(P)_2\text{-6}$ were also solved, in the space groups $C222_1$ ($0.5\text{CH}_2\text{Cl}_2$) and $P6_122$ (MeCN; for all crystal structures, see Section S5 in the Supporting Information). The asymmetric unit of $C222_1$ contains two halves of each dimeric unit due to crystallographic symmetry. The thiophene sulfur of the first dimer, with a nearby CH_2Cl_2 molecule ($d(\text{S} \cdots \text{Cl}) = 3.7$ Å, angle $\text{Cl} \cdots \text{S} - \text{C} = 117^\circ$), is located on a 2_1 axis, whereas the thiophene of the second dimer rests on a 2 axis. The torsional angles between the linked benzene rings of the helicenes are 22° and 41° , respectively (Figure 5). Terminal benzene rings of neighboring dimers come close, yielding even a repulsive contact at $d(\text{C} \cdots \text{C}) = 3.1$ Å. The second solvomorph (space group $P6_522$) shows a close S-contact ($d(\text{S} \cdots \text{N}) = 3.7$ Å) to the MeCN solvate molecule (which is disordered about a twofold axis; see Section S4 in the Supporting Information). The molecular geome-

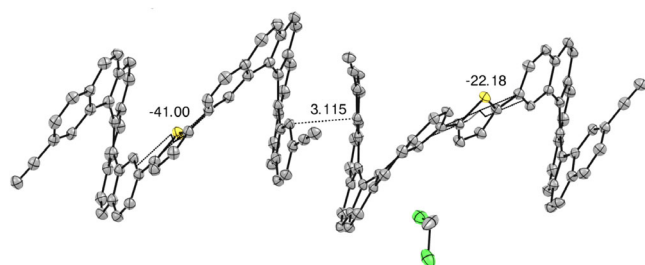


Figure 5. ORTEP plots of $(M)_2\text{-6} \cdot 0.5\text{CH}_2\text{Cl}_2$ in $C222_1$. Hydrogen atoms have been omitted for clarity. Atomic displacement parameters at 100 K are drawn at the 50% probability level. For further information on bond lengths [Å] and torsions [$^\circ$], see the Supporting Information.

tries of the thiene-2,5-diyl-linked dimers were nicely reproduced by DFT calculations (DFT:B3LYP/6-31G(d)).^[9]

In conclusion, a synthetic route to enantiopure 2,15-bis[(triisopropylsilyl)ethynyl]carbo[6]helicenes $(P)\text{-3}$ and $(M)\text{-3}$ in 25% yield over 6 steps, followed by optical resolution by HPLC on a chiral stationary phase was reported. Monodeprotection followed by oxidative acetylenic coupling afforded buta-1,3-diyne-1,4-diyl-linked dimeric [6]helicenes $(P)_2\text{-1}$ and $(M)_2\text{-1}$ and subsequently tetrameric $(P)_4\text{-2}$ and $(M)_4\text{-2}$. The tetrameric oligomers display large Cotton effects in ECD spectroscopy. The differences in the increase of the chiroptical properties upon moving from monomeric to dimeric and tetrameric systems were explained by DFT calculations and correlated with the extension of π -electron delocalization. We also prepared the thiene-2,5-diyl-linked dimeric $(P)_2\text{-6}$ and $(M)_2\text{-6}$ which feature a strong fluorescence intensity, a desirable but rare property of carbo[*n*]helicenes. Monomeric and dimeric helicenes were characterized by extensive X-ray analysis showing a remarkable tendency of the dimeric chromophores to form solvo- and polymorphs, allowing for confirmation of the conformations predicted by DFT calculations. Other heteroarene-linked dimeric helicenes are currently under preparation.

Acknowledgements

This work was supported by a grant from the Swiss National Science Foundation (SNF 200020_159802). The authors thank Michael Solar for his support with X-Ray crystallography and Anatol Schwab for help with the HPLC separation. We thank Dr. Bruno Bernet for corrections of the synthetic protocols and spectral characterizations. Dr. Nicolas Kerisit and Raoul De Gasparo are acknowledged for fruitful discussions, Leslie Riwar, Geoffrey Schwartz, and Brendan Quigley for proofreading the manuscript.

Conflict of interest

The authors declare no conflict of interest.

Keywords: circular dichroism · helicenes · oligomerization · photocyclodehydrogenation · π -electron delocalization · polymorphism

- [1] a) R. H. Martin, *Angew. Chem. Int. Ed. Engl.* **1974**, *13*, 649–660; *Angew. Chem.* **1974**, *86*, 727–738; b) R. H. Martin, M. Baes, *Tetrahedron* **1975**, *31*, 2135–2137; c) A. Urbano, *Angew. Chem. Int. Ed.* **2003**, *42*, 3986–3989; *Angew. Chem.* **2003**, *115*, 4116–4119; d) M. Gingras, *Chem. Soc. Rev.* **2013**, *42*, 968–1006; e) C.-F. Chen, Y. Shen, *Helicene Chemistry. From Synthesis to Applications*, Springer, Berlin, **2017**.
- [2] a) R. H. Martin, M. Flammang-Barbier, J. P. Cosyn, M. Gelbcke, *Tetrahedron Lett.* **1968**, *9*, 3507–3510; b) R. H. Martin, G. Morren, J. J. Schurter, *Tetrahedron Lett.* **1969**, *10*, 3683–3688; c) H. Kagan, A. Moradpour, J. F. Nicoud, G. Balavoine, R. H. Martin, J. P. Cosyn, *Tetrahedron Lett.* **1971**, *12*, 2479–2482; d) P. Sehnal, I. G. Stará, D. Šaman, M. Tichý, J. Mišek, J. Cvačka, L. Rulišek, J. Chocholeušová, J. Vacek, G. Goryl, M. Szymonski, I. Císařová, I. Starý, *Proc. Natl. Acad. Sci. USA* **2009**, *106*, 13169–13174.
- [3] K. Mori, T. Murase, M. Fujita, *Angew. Chem. Int. Ed.* **2015**, *54*, 6847–6851; *Angew. Chem.* **2015**, *127*, 6951–6955.

- [4] a) T. Fujikawa, Y. Segawa, K. Itami, *J. Am. Chem. Soc.* **2016**, *138*, 3587–3595; b) X.-Y. Wang, X.-C. Wang, A. Narita, M. Wagner, X.-Y. Cao, X. Feng, K. Müllen, *J. Am. Chem. Soc.* **2016**, *138*, 12783–12786; c) A. Pradhan, P. Dechambenoit, H. Bock, F. Durolo, *Chemistry* **2016**, *22*, 18227–18235; d) Y. Hu, X.-Y. Wang, P.-X. Peng, X.-C. Wang, X.-Y. Cao, X. Feng, K. Müllen, A. Narita, *Angew. Chem. Int. Ed.* **2017**, *56*, 3374–3378; *Angew. Chem.* **2017**, *129*, 3423–3427.
- [5] a) K. Nakamura, H. Okubo, M. Yamaguchi, *Org. Lett.* **2001**, *3*, 1097–1099; b) Y. Saiki, K. Nakamura, Y. Nigorikawa, M. Yamaguchi, *Angew. Chem. Int. Ed.* **2003**, *42*, 5190–5192; *Angew. Chem.* **2003**, *115*, 5348–5350; c) H. Sugiura, Y. Nigorikawa, Y. Saiki, K. Nakamura, M. Yamaguchi, *J. Am. Chem. Soc.* **2004**, *126*, 14858–14864; d) Y. Kushida, N. Saito, M. Shigeno, M. Yamaguchi, *Chem. Sci.* **2017**, *8*, 1414–1421.
- [6] J. Roose, S. Achermann, O. Dumele, F. Diederich, *Eur. J. Org. Chem.* **2013**, 3223–3231.
- [7] a) H. Wynberg, *Acc. Chem. Res.* **1971**, *4*, 65–73; b) T. Caronna, R. Sinisi, M. Catellani, L. Malpezzi, S. V. Meille, A. Mele, *Chem. Commun.* **2000**, 1139–1140; c) E. Mena-Osteritz, A. Meyer, B. M. W. Langeveld-Voss, R. A. J. Janssen, E. W. Meijer, P. Bäuerle, *Angew. Chem. Int. Ed.* **2000**, *39*, 2679–2684; *Angew. Chem.* **2000**, *112*, 2791–2796; d) Q. Zheng, R. Hua, J. Jiang, L. Zhang, *Tetrahedron* **2014**, *70*, 8252–8256; e) M. Iyoda, H. Shimizu, *Chem. Soc. Rev.* **2015**, *44*, 6411–6424.
- [8] a) F. Furche, R. Ahlrichs, C. Wachsmann, E. Weber, A. Sobanski, F. Vögtle, S. Grimme, *J. Am. Chem. Soc.* **2000**, *122*, 1717–1724; b) G. Portella, J. Poater, J. M. Bofill, P. Alemany, M. Solà, *J. Org. Chem.* **2005**, *70*, 2509–2521; c) Y. Nakai, T. Mori, Y. Inoue, *J. Phys. Chem. A* **2012**, *116*, 7372–7385; d) Y. Nakai, T. Mori, Y. Inoue, *J. Phys. Chem. A* **2013**, *117*, 83–93.
- [9] Gaussian 09, Revision A.02, M. J. Frisch, G. W. Trucks, H. B. Schlegel, G. E. Scuseria, M. A. Robb, J. R. Cheeseman, G. Scalmani, V. Barone, G. A. Petersson, H. Nakatsuji, X. Li, M. Caricato, A. Marenich, J. Bloino, B. G. Janesko, R. Gomperts, B. Mennucci, H. P. Hratchian, J. V. Ortiz, A. F. Izmaylov, J. L. Sonnenberg, D. Williams-Young, F. Ding, F. Lipparini, F. Egidi, J. Goings, B. Peng, A. Petrone, T. Henderson, D. Ranasinghe, V. G. Zakrzewski, J. Gao, N. Rega, G. Zheng, W. Liang, M. Hada, M. Ehara, K. Toyota, R. Fukuda, J. Hasegawa, M. Ishida, T. Nakajima, Y. Honda, O. Kitao, H. Nakai, T. Vreven, K. Throssell, J. A. Montgomery, Jr., J. E. Peralta, F. Ogliaro, M. Bearpark, J. J. Heyd, E. Brothers, K. N. Kudin, V. N. Staroverov, T. Keith, R. Kobayashi, J. Normand, K. Raghavachari, A. Rendell, J. C. Burant, S. S. Iyengar, J. Tomasi, M. Cossi, J. M. Millam, M. Klene, C. Adamo, R. Cammi, J. W. Ochterski, R. L. Martin, K. Morokuma, O. Farkas, J. B. Foresman, D. J. Fox, Gaussian, Inc., Wallingford CT, **2016**.
- [10] a) L. Norel, M. Rudolph, N. Vanthuyne, J. A. G. Williams, C. Lescop, C. Roussel, J. Autschbach, J. Crassous, R. Réau, *Angew. Chem. Int. Ed.* **2010**, *49*, 99–102; *Angew. Chem.* **2010**, *122*, 103–106; b) D. Schweinfurth, M. Zalibera, M. Kathan, C. Shen, M. Mazzolini, N. Trapp, J. Crassous, G. Gscheidt, F. Diederich, *J. Am. Chem. Soc.* **2014**, *136*, 13045–13052.
- [11] CCDC 1552906–1552916 contain the supplementary crystallographic data for this paper. These data can be obtained free of charge from The Cambridge Crystallographic Data Centre.
- [12] R. Rossi, A. Carpita, C. Bigelli, *Tetrahedron Lett.* **1985**, *26*, 523–526.
- [13] H. B. Klevens, J. R. Platt, W. C. Prize, *J. Chem. Phys.* **1949**, *17*, 466–469.
- [14] H. Isla, M. Srebro-Hooper, M. Jean, N. Vanthuyne, T. Roisnel, J. L. Lunkley, G. Muller, J. A. G. Williams, J. Autschbach, J. Crassous, *Chem. Commun.* **2016**, *52*, 5932–5935.
- [15] a) J. B. Birks, D. J. S. Birch, E. Cordemans, E. Vander Donckt, *Chem. Phys. Lett.* **1976**, *43*, 33–36; b) H. Oyama, K. Nakano, T. Harada, R. Kuroda, M. Naito, K. Nobusawa, K. Nozaki, *Org. Lett.* **2013**, *15*, 2104–2107; c) H. Sakai, S. Shinto, J. Kumar, Y. Araki, T. Sakanoue, T. Takenobu, T. Wada, T. Kawai, T. Hasobe, *J. Phys. Chem. C* **2015**, *119*, 13937–13947; d) T. Hirose, N. Ito, H. Kubo, T. Sato, K. Matsuda, *J. Mater. Chem. C* **2016**, *4*, 2811–2819.
- [16] C. Würth, M. Grabolle, J. Pauli, M. Spieles, U. Resch-Genger, *Nat. Protocols* **2013**, *8*, 1535–1550.
- [17] T. Michinobu, C. Boudon, J.-P. Gisselbrecht, P. Seiler, B. Frank, N. N. P. Moonen, M. Gross, F. Diederich, *Chem. Eur. J.* **2006**, *12*, 1889–1905.

Manuscript received: June 30, 2017

Accepted manuscript online: ■■■■■, 0000

Version of record online: ■■■■■, 0000

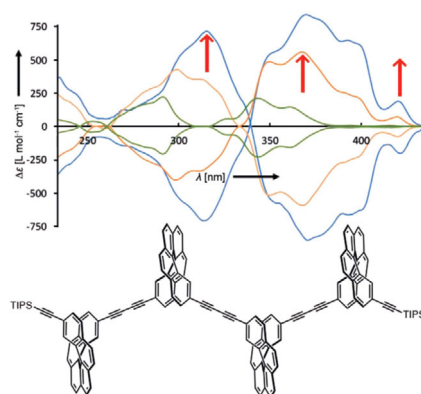
COMMUNICATION

Synthetic Methods

C. Schaack, E. Sidler, N. Trapp,
F. Diederich*



Helical Threads: Enantiomerically Pure Carbo[6]Helicene Oligomers



Bigger, better! An efficient route to enantiopure 2,15-dialkynylated carbo[6]-helicenes and buta-1,3-diyne-1,4-diyl- and thiene-2,5-diyl-linked dimeric and tetrameric oligomers is described. The chiroptical properties are correlated with the extent of π -electron delocalization. X-ray analysis provided conformational information consistent with DFT-calculated structures. The thiene-2,5-diyl-bridged dimers display intense fluorescence emission, which is a rare property in carbohelicene chemistry (see scheme).